The application of infrared spectroscopy to probe the surface morphology of alumina-supported palladium catalysts

Timothy Lear, Robert Marshall, J. Antonio Lopez-Sanchez, and S. David Jackson
Department of Chemistry, Joseph Black Building, University of Glasgow, Glasgow G12 8QQ, Scotland, United Kingdom

Thomas M. Klapötke
Department of Chemistry and Biochemistry, Ludwig-Maximilian University of Munich, Butenandtstrasse 5-13 (Haus D), D-81377 Munich, Germany

Marcus Bäumer, Günther Rupprechter, and Hans-Joachim Freund
Fritz-Haber-Institut der Max-Planck-Gesellschaft, Chemical Physics Department, Faradayweg 4-6, D-14195 Berlin, Germany

David Lennon[a)]
Department of Chemistry, Joseph Black Building, University of Glasgow, Glasgow G12 8QQ, Scotland, United Kingdom

(Received 28 June 2005; accepted 6 September 2005; published online 1 November 2005)

Five alumina-supported palladium catalysts have been prepared from a range of precursor compounds [palladium(II) nitrate, palladium(II) chloride, palladium(II) acetylacetonate, and tetraamminepalladium(II) tetraazidopalladate(II)] and at different metal loadings (1–7.3 wt %). Collectively, this series of catalysts provides a range of metal particle sizes (1.2–8.5 nm) that emphasize different morphological aspects of the palladium crystallites. The infrared spectra of chemisorbed CO applied under pulse-flow conditions reveal distinct groupings between metal crystallites dominated by low index planes and those that feature predominantly corner/edge atoms. Temperature-programmed infrared spectroscopy establishes that the linear CO band can be resolved into contributions from corner atoms and a combination of (111)/(111) and (111)/(100) particle edges. Propene hydrogenation has been used as a preliminary assessment of catalytic performance for the 1 wt % loaded catalysts, with the relative inactivity of the catalyst prepared from palladium(II) chloride attributed to a diminished hydrogen supply due to decoration of edge sites by chlorine originating from the preparative process. It is anticipated that refinements linking the vibrational spectrum of a probe molecule with surface structure and accessible adsorption sites for such a versatile catalytic substrate provide a platform against which structure/reactivity relationships can be usefully developed. © *2005 American Institute of Physics*. [DOI: 10.1063/1.2101487]

I. INTRODUCTION

A "holy grail" in heterogeneous catalysis is to develop structure-activity relationships, where the catalyst structure is controlled via preparative procedures to reproducibly yield catalysts of defined structure that favor specific chemical pathways.[1–5] Concentrating on supported metal catalysts applied to hydrogenation reactions,[6] this approach requires a knowledge of the metal crystallite structure. This is achievable in favorable circumstances by the application of high-resolution transmission electron microscopy[7] but this powerful technique cannot be universally applied to a range of catalysts, requires detailed analysis, and commonly examines the catalyst in the absence of any reacting gases, which could induce reconstructions of the metal surface.[8] An alternative approach to the problem is to use vibrational spectroscopy, most commonly infrared spectroscopy,[9] to monitor how probe molecules such as CO are perturbed upon adsorption on the metal crystallites.[10] Then, from an appreciation of the vibrational frequency of the probe molecule in defined coordination geometries, often obtained via application of the metal cluster-surface analogy,[11] the form of the metal sites available for adsorption, and hence reaction, can be deduced.[12] In the majority of cases it is possible to access the vibrational information but it tends to be much harder to establish the catalyst structural information. Over the last 30 years or so metal single crystals have been used to bridge this knowledge gap. These substrates start with the distinct advantage that the surface structure is well defined and, when studied in an ultrahigh-vacuum (UHV) environment, tools such as low-energy electron diffraction combined with reflection absorption infrared spectroscopy[13] or vibrational electron energy-loss spectroscopy[14] can be used to determine the adsorbate structure. This favorable overlap between surface science and heterogeneous catalysis has provided considerable insight as to which metal sites are active for chemisorption and reaction. This topic has been comprehensively reviewed by several authors, e.g., Refs. 10, 15, and 16.

However, it is noted that the vibrational spectra for the metal single crystals do not always match that observed for

[a)]Author to whom correspondence should be addressed. Fax: (+44)-(0)-141-330-4888. Electronic mail: d.lennon@chem.gla.ac.uk

the high surface area supported metal catalyst. For example, the pioneering spectra of Eischens *et al.* for high coverages of CO on Pd/SiO_2 at room temperature show a linear CO feature about 2060 cm^{-1} and a dominant broad region of absorption between 1700 and 1950 cm^{-1}, which is attributed to various bridge-bonded species.[15,17] This spectral profile has been observed many times for a wide variety of supported Pd catalysts.[15,18–20] In contrast, for CO on Pd(111) and (100),[21] linear CO makes a minor contribution at 300 K and is normally only observable in the presence of an overpressure of CO.[22] Kuhn *et al.* have produced an equilibrium pressure-temperature phase diagram for Pd(111)/CO, which demonstrates the importance of sample preparation conditions and the manner in which spectra are recorded.[23] The picture is further complicated when one examines highly dispersed Pd catalysts having mean metal sizes <2 nm. In these cases the spectrum of chemisorbed CO is characterized by an abnormally strong linear CO band between 2070 and 2110 cm^{-1}, relative to the bridged CO bands.[24,25] Additionally, this latter group of catalysts is thought to be sensitive to support effects.[26] Finalizing the comments related to metal single crystals (surface area ca. 1 cm^2) acting as models in heterogeneous catalysis, it is also noted that meaningful comparisons between conventional catalytic measurements made even at modest temperatures (300 K) and pressures (1 atm) on the high surface area catalysts [metal surface area ca. 2 m^2/g (Ref. 27)] are a nontrivial business.[28]

Within the last ten years or so, considerable advances in model systems relevant to heterogeneous catalysis have occurred as a result of modern surface science techniques being able to prepare and characterize dispersed metal crystallites on realistic mimics for catalyst support materials such as silica[29–31] or alumina.[32–36] The infrared spectra of adsorbates and probe molecules are accessible on these substrates,[34] as are other techniques such as temperature-programmed desorption (TPD).[37] Most importantly, such substrates are amenable to investigation by scanning tunneling microscopy (STM), which means that the surface structure at the atomic level can be determined, making correlations between surface chemistry and surface structure a realistic proposition. This subject has been reviewed[30,32,33] and considerable advancements have been made for a number of catalytic systems, including Pd/Al_2O_3.[38] Nevertheless, such small surface area substrates are still hindered by the fact that they tend to be contained within an UHV environment, restraining comparable chemical reactivity measurements to those performed in a conventional catalytic microreactor. Sum frequency generation techniques coupled with an ancillary pressure cell represent an exception to this situation,[39–41] although it is noted that such hardware and expertise are rarely available in traditional heterogeneous catalysis laboratories.

An alternative approach is to examine metal nanoparticles on support materials that favor well-ordered metal crystallites. For example, Bertarione *et al.* have recently examined CO adsorption on Pd nanoparticles supported on MgO.[42] These materials yield distinct chemisorbed CO infrared spectra that indicate a high degree of order within the Pd particles. That work has been extended to examine the issues of methanol adsorption on these catalysts.[43] Whereas MgO has a relatively minor application in industrial heterogeneous catalysis, investigations on alumina-supported palladium catalysts [alumina is thought to be the most widely used commercial carrier (support) material[44,45]] show a high level of defects and disorder in the palladium particles,[42] restricting their usefulness in correlating specific facets with observed activity. Against this background, the authors have recently developed a novel preparative procedure for preparing residue-free, high surface area alumina-supported palladium catalysts that present a well-defined palladium morphology.[46] The vibrational spectrum of the adsorbed probe molecules of this "benchmark" material can then be compared with a range of catalysts and the connection to catalyst morphology examined. This communication uses diffuse reflectance infrared spectroscopy, an ideal probe for *operando* (or *in situ*) studies of heterogeneously catalyzed reaction systems,[1,3,47] to investigate CO adsorption on a range of industrial specification alumina-supported palladium catalysts prepared from a variety of precursor compounds [palladium(II) nitrate, palladium(II) chloride, palladium(II) acetylacetonate, and tetraamminepalladium(II) tetraazidopalladate(II) (Ref. 48)]. This suite of catalysts covers a broad range of particle sizes (1.2–8.5 nm) that emphasizes different morphological aspects of the palladium crystallites. Degussa Oxid C was selected as the support material in all instances, as it is commonly used in the manufacture of heterogeneous catalysts. It is a highly dispersed fumed aluminium oxide exhibiting high purity (Al_2O_3 content $\geqslant$99.60 wt %).[49] Vibrational assignments confirmed by examination of model systems[32,33,50,51] are then used to describe the active site distributions of the catalysts studied. Furthermore, application of pulse-flow methods to control adsorbate exposures restricts the population of certain adsorption geometries and provides some advantages over the more conventional equilibrium-based methods. Specifically, in the absence of an equilibrium pressure of CO, adsorption of CO into on-top sites does not occur to any significant degree on palladium surfaces dominated by low index planes.[21,52] However, this feature can dominate the spectrum when there is a high density of corner atoms, as typically encountered on highly dispersed catalysts. Thus, this synthetic and spectroscopic approach to a mature problem has the potential to provide extra insight into how different preparative procedures could be used to influence catalytic performance by modifying the surface structure of the metal crystallites, which ultimately controls the chemical transformations associated with these type of catalysts.

The Pd/alumina system was selected for investigation because (i) it has a wide application in heterogeneous catalysis,[53,54] (ii) there is a substantial database of model systems,[32,33,35,55] and (iii) the CO adsorbate structure on this surface is well characterized over a wide range of conditions. This latter point has recently been examined in some detail by sum frequency generation vibrational spectroscopy, which establishes that the CO resides in "regular" adsorption sites over a wide pressure range (10^{-8}–1000 mbars).[52,56–58] Such an appreciation of the bonding options and their assignments

TABLE I. Summary of catalyst characterization details. With the exception of the 1% $Pd(NO_3)_2$/alumina catalyst, all samples were examined for C, H, N, and Cl by elemental analysis, with only positive values included in the table. CO chemisorption saturation values were performed at 293 K. The errors represent the standard deviation from a number of replicate experiments. Mean particle size is calculated according to Eq. (1). Mean particle sizes for the palladium crystallites via TEM are only available for the Pd(azide) and 5% $Pd(NO_3)_2$ catalysts; metal particles were not discernible with the other catalysts.

Catalyst	Pd loading (wt %)	B.E.T. ($m^2\ g^{-1}$)	Elemental analysis (wt %)	Saturation coverage of CO (μmol CO $g^{-1}_{(cat)}$)	Catalyst dispersion (%)	Calculated Pd mean particlesize (nm)	Observed Pd particle size (TEM) (nm)
10% Pd(azide)/alumina	7.3	94	···	45	13	8.5	ca. 10
5% $Pd(NO_3)_2$/alumina	4.0	102.6	0.8% N	90.9±15	48±8	2.3	2.5±1.0
1% $PdCl_2$/alumina	0.91	70.9	5.4% Cl	19.5±1.4	46±3	2.5	···
1% $Pd(NO_3)_2$/alumina	0.86	104.4	N/A	32.0±0.42	79±1	1.4	···
1% Pd(acac)/alumina	0.93	100.8	0.7% C	42.4±0.75	97±2	1.2	···

on model systems aids greatly the interpretation of the results obtained on more complex, but more technologically useful, high surface substrates.

In order to provide an indication of the viability of the catalysts studied, some results for propene hydrogenation[59] performed under continuous flow conditions are also presented. These demonstrate a range of reaction profiles and demonstrate the catalyst prepared from palladium chloride to exhibit the lowest activity. With reference to the chemisorbed CO infrared studies, which indicate the presence of chlorine residues on both low index planes and edge atoms of the palladium crystallites, the relatively low activity is attributed to chlorine residues at the edge atom sites, restricting hydrogen supply by reducing the opportunities for dissociative hydrogen adsorption. In this manner, infrared spectroscopy can be used as an indirect probe of surface structure and accessible adsorption sites, so providing a platform against which structure/reactivity relationships can be usefully developed.

II. EXPERIMENT

A. Catalyst preparation and characterization

Three palladium alumina catalysts with a 1 wt % loading were prepared using the following precursors, palladium(II) chloride ($PdCl_2$, Aldrich, 99.999%), palladium(II) acetylacetonate [Pd(acac), Aldrich, 99%], and palladium(II) nitrate [$Pd(NO_3)_2$, Alfa Aesar, 99.9%]. The catalysts were prepared by an impregnation method as follows. Aluminiumoxid C (Degussa), Brunauer-Emmett-Teller (B.E.T) surface area 106 $m^2\ g^{-1}$, was weighed out into a 2 liter round bottom flask, into which the required solvent was added; dilute HCl for $PdCl_2$, toluene for Pd(acac), and water for $Pd(NO_3)_2$. Once a slurry of alumina and solvent was obtained, the calculated amount of precursor was dissolved into the minimum amount of solvent and added dropwise into the round bottom flask, stirring continuously. This mixture was left to stir for 24 h, after which the solvent was removed using a rotary evaporator. The resulting mixture was dried in an oven at 373 K overnight and the subsequent mixture sieved into particles in the range of 250–500 μm. This material was then calcined in air at 473 K for 1 h. The 5 wt % $Pd(NO_3)_2$/alumina was prepared in a similar fashion.

For reference purposes, an additional 10 wt % alumina-supported palladium catalyst was also examined. This was prepared by using a controlled explosion to combine the unstable precursor tetraamminepalladium(II) tetraazidopalladate(II) (Ref. 48) with the same support material as used for the impregnated catalysts. This hazardous preparative route has been described elsewhere[46] and results in a residue-free catalyst with a well-defined metal crystallite surface morphology. The catalyst is hitherto described as Pd(azide)/alumina.

Characterization of the five catalyst samples is presented in Table I. The Pd content was quantified by atomic absorption spectrophotometry using a Perkin Elmer 1100B atomic absorption spectrophotometer. Nitrogen BET chemisorption measurements were performed using a Micromeritics ASAP 2400 surface area analyzer. With the exception of the $PdCl_2$/alumina sample, the total surface area of the prepared catalysts did not unduly differ from that of the support material. The requirement to use HCl to aid the dissolution of $PdCl_2$ is thought to be responsible for the reduced surface area seen with this catalyst. Elemental analysis for C, H, N, and Cl was performed using a CE-440 elemental analyzer on unreduced samples. The alumina support gave a background level of carbon of <0.3 wt. %. The palladium(II) nitrate and palladium(II) acetylacetonate catalysts contained modest residues of nitrogen and carbon, respectively. However, the $PdCl_2$/alumina sample contained chlorine at a value of 5.4 wt %. Evidently, the combination of a chloride salt and the use of HCl in the preparation stage result in the retention of substantial quantities of halide with this catalyst. Transmission electron microscopy (JOEL 1200 FX electron microscope operating at an acceleration voltage of 120 kV) was used to evaluate the particle size of the palladium crystallites. Adsorption isotherms for carbon monoxide (Linde Gas, 99.95% purity) chemisorption were performed using a pulse-flow technique,[27] utilizing a thermal-conductivity detector housed within a Philips PU 4500 gas liquid chromatograph. The catalysts were activated prior to chemisorption studies

by passing a 6% H_2/N_2 mixture (BOC, 99.995% purity) over the samples at a flow rate of 30 ml min^{-1}, while effecting a linear temperature ramp of 3 K min^{-1} from 293 to 473 K. The temperature was maintained at 473 K for 30 min, then the flowing gas switched to helium (BOC, 99.995% purity) with the sample maintained at the elevated temperature for 30 min in order to remove excess hydrogen. The sample was then allowed to cool to ambient temperature under a continuous flow of helium.[6] The purity of the incoming gases was ensured by in-line drying (activated molecular sieve) and deoxygenating (Messer Greisheim Oxysorb) agents.

B. Infrared spectroscopy

Infrared experiments were performed using a Nicolet Nexus Fourier transform infrared (FTIR) spectrometer fitted with a mercury cadmium telluride (MCT) high D^* detector. Measurements were performed in diffuse reflectance mode using a SpectraTech Smart diffuse reflectance cell and environmental chamber, using a known sample mass of ca. 20 mg of catalyst. The cell was connected to a vacuum manifold/gas flow apparatus that provides control of the flow of gases into the infrared cell. This includes an in-line sample loop for sequential dosing of the catalyst in a pulse-flow arrangement. The exit stream of the infrared cell could be monitored by either a gas liquid chromatograph (Philips PU 4500) or a quadrupole mass spectrometer (LedaMass LM22). A constant stream of high-purity helium was passed over the catalyst at all times (30 ml min^{-1}, 1.5 atm). The samples were activated *in situ* using the same procedures outlined for the pulse chemisorption experiments. Background spectra were recorded post-activation at 293 K. Carbon monoxide (Linde Gas, 99.95% purity) was dosed on to the catalyst at 293 K using pulse-flow techniques.[6,60] The magnitude of the pulse size used was dependent on the saturation capacity of each catalyst. Two pulse sizes were used throughout: 13 and 65 μmol CO g_{cat}^{-1}. The geometric arrangement of the cell meant that dosing was associated with a substantial degree of gas bypass. Ancillary experiments confirmed that a 5 min delay after each dosing pulse was sufficient time for the adsorbate to be completely removed from the environmental chamber. After dosing, the spectrum was recorded (512 scans, resolution of 4 cm^{-1}). All spectra are presented as background subtractions, where a spectrum of the activated catalyst has been subtracted from the dosed spectrum. No base line or offset corrections were made. For carbon monoxide desorption experiments, the cell containing the predosed catalyst sample was heated under flowing He. The cell was maintained at a specified temperature for 10 min, before being cooled to room temperature when a spectrum was recorded. Separate CO temperature-programmed desorption experiments using a tubular reactor, furnace, and mass spectrometer were also performed on all of the catalysts[61] and established that the infrared desorption profiles were representative of those expected from conventional gas-phase analysis, e.g., Ref. 62.

C. Propene hydrogenation

Approximately 10 mg of the catalyst were packed into a 2-mm-i.d. stainless-steel reactor that was housed in a programmable furnace. Mass flow controllers (Brooks 5850S) ensured reproducible gas concentrations. Helium and hydrogen (BOC, 99.99% purity) were purified using in-line deoxygenating and drying traps. The propene (Linde, 99% purity) was used without further purification. Propane (Linde, 99% purity) was used for gas chromatographic calibration. The catalysts were activated as described above. Reactions were performed at 298 K and 2 bar pressure with respective hydrogen, propene, and helium flow rates of 10, 10, and 80 ml min^{-1}. This equimolar hydrogen: propene mixture equates to a propene flow rate of 2.96×10^{20} propene molecules min^{-1}. Product distributions were analyzed by on-line gas chromatography mass spectrometry (GC-MS) (Hewlett Packard GC6890 fitted with a 25 m $\times$ 4 μm CP-Al_2O_3/KCl column and equipped with a Hewlett Packard 5973 mass selective detector), sampling via an automated gas sampling valve. Varying the catalyst mass and gas linear velocity confirmed the absence of diffusional effects under operating conditions.

III. RESULTS AND DISCUSSION

This section is comprised as follows. Firstly, Sec. III A describes the outcome from a series of adsorption isotherm and electron microscopic investigations that provide information on the particle size of the palladium crystallites for the five catalysts studied. The chemisorption of carbon monoxide is then examined by means of diffuse reflectance infrared spectroscopy in Sec. III B, where the spectra are presented as a function of (a) increasing CO exposure and (b) progressive thermally induced desorption of a saturated overlayer of CO. Sec. III C summarizes the vibrational spectra observed. Finally, Sec. III D briefly considers the issue of associated catalytic activity using propene hydrogenation as a test reaction.

A. Adsorption isotherms and transmission electron microscopy

The palladium content of each of the five catalysts as determined by atomic absorption spectrophotometry is presented in Table I. The loadings are all on the low side of the target weights, indicating inefficiencies in the preparative procedures. The alumina support material was shown to contain no palladium. CO adsorption isotherms were performed using a pulse-flow technique[27] and saturation values are presented in Table I. The concentration of surface palladium atoms can be determined assuming a surface stoichiometry of CO:Pd(s=1:2).[63] The corresponding dispersion values are included in Table I. Assuming the metal particles to be spherical,[27] particle sizes (d,m) can be calculated from the dispersion values $(D,\%/100)$ using the following equation:

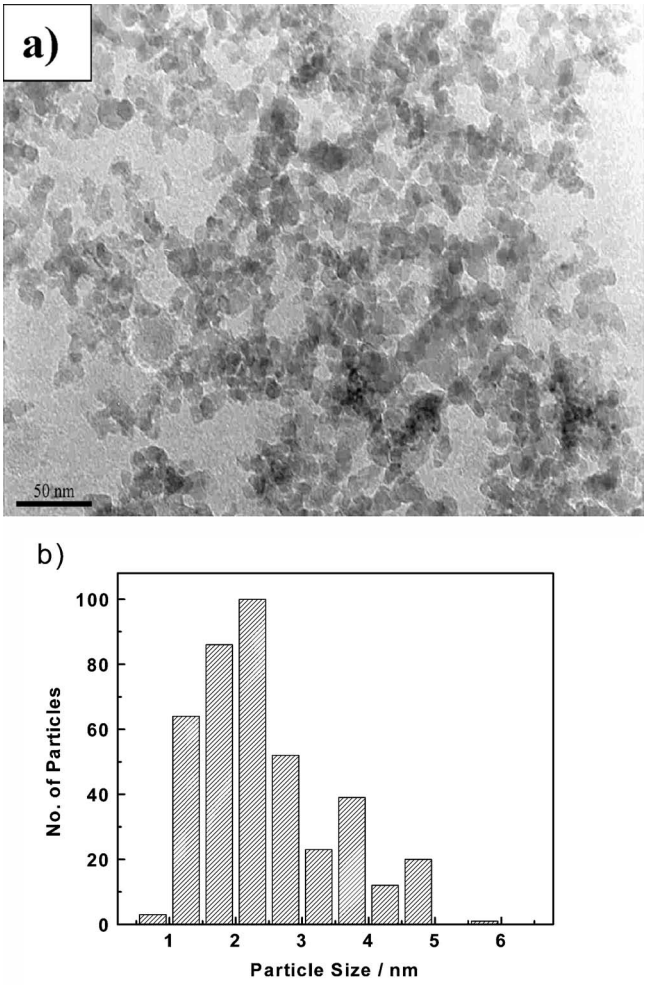

FIG. 1. Transmission electron microscopy for the 5% $Pd(NO_3)_2/Al_2O_3$ catalyst: (a) micrograph showing nanometer-size palladium particles well distributed over the alumina support; (b) particle size distribution histogram.

$$d = \frac{6A}{\rho\sigma LD}, \tag{1}$$

where A=atomic mass (106.42 g mol^{-1}), ρ=density (12.02×10^6 g m^{-3}), σ=average surface area occupied by one Pd atom ($(0.79 \times 10^{-19}$ m^2), and L=Avogadro's constant.[20,27,64] The resulting mean particle sizes are also presented in Table I. All of the catalysts were examined by a JOEL 1200 FX transmission electron microscope (TEM). However, metal particles were only observable with the Pd(azide)/alumina and 5% $Pd(NO_3)_2$/alumina catalysts. Previous measurements using this microscope have demonstrated difficulties in distinguishing Pd particles from alumina when the particles are $\leqslant$3 nm. Therefore, it is assumed that the 1% $Pd(NO_3)_2$, 1% $PdCl_2$, and 1% Pd(acac) catalysts have mean particle of sizes $<$3 nm. The TEM studies on the Pd(azide)/alumina catalyst are described elsewhere[46] and indicate particles exhibiting a hexagonal structure, which can be described in terms of low index planes, i.e., (111) and (100), with a low level of surface defects. The dominance of low index planes is partially a consequence of the high annealing temperature of 873 K used for this catalyst. Complete thermal decomposition of the azide precursor can be achieved at lower anneal temperatures and future work will explore the linkage between activation procedure and crystallite morphology in more detail. A representative electron micrograph for the 5% $Pd(NO_3)_2$/alumina catalyst is shown in Fig. 1(a), and Fig. 1(b) shows the particle size distribution to be gently skewed to larger-diameter particles. The mean particle size for both of these samples is presented in Table I. For the other catalysts, the particle size was assumed to be too small to be detected by this instrument, demonstrating the importance of the chemisorption measurements. In the case of the Pd(azide)/alumina and the 5% $Pd(NO_3)_2$/alumina catalysts for which both TEM and chemisorption data are available, Table I shows the agreement between calculated and mean particle size to be reasonable. Summarizing, Table I shows that the five alumina-supported palladium catalysts prepared from a series of precursor compounds have palladium particle sizes ranging from 1.2 to 8.5 nm which, assuming spherical particles, approximate to palladium crystallites containing 4–30 atoms across the diameter of the particle.

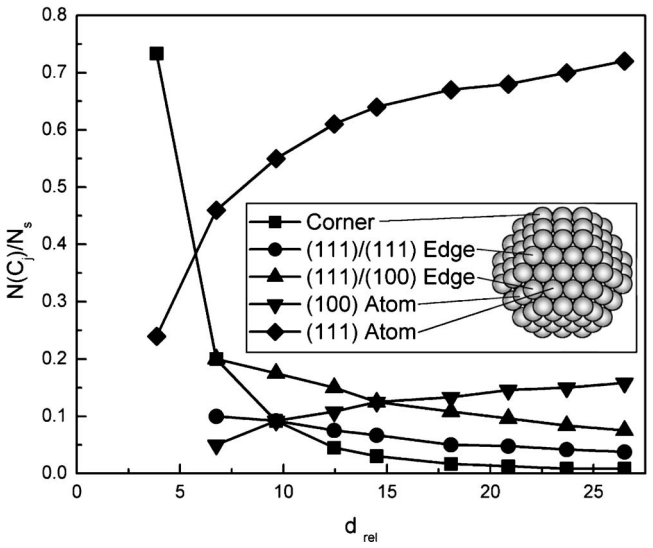

FIG. 2. Distribution of the number of atoms on corners, edges, and planes divided by the total number of surface atoms vs the relative diameter of the metal particle. The figure is redrawn with permission from Elsevier from two illustrations contained within Ref. 24.

Supported catalyst particles are usually well described by simple geometric structures such as spheres or hemispheres.[27] TEM shows the Pd(azide)/alumina catalyst to be comprised of particles, some of which exhibit a distinct hexagonal structure, consistent with cubo-octahedra.[46] van Hardeveld and Hartog established the relationship between metal particle size and crystallite morphology.[24] More recently, Schimpf *et al.* have used such concepts to evaluate the structure/activity relationships for supported gold catalysts applied to selective hydrogenation reactions.[65] Investigations on model alumina-supported palladium catalysts have been able to refine the description of adsorption sites on well-defined nanoparticles.[32,33] Following this approach, Fig. 2 illustrates the relative distribution of the most relevant adsorption sites for an idealized Pd particle as a function of particle diameter. Figure 3 extends this concept by illustrating a schematic representation of the Pd particles for all five catalysts. The selection of the particle shape has been guided

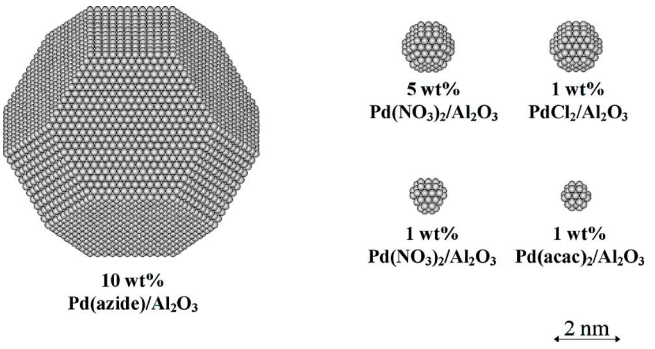

FIG. 3. Schematic representation of the palladium crystallites for the five Pd/Al_2O_3 catalysts described in the text. Mean particle size has been determined from CO chemisorption measurements and electron microscopy in favorable circumstances. Particle shape is assumed to approximate to a cubo-octahedron.

by TEM studies of the Pd(azide) catalyst.[46] A cubo-octahedron is used to describe the Pd(azide)/alumina catalyst and clearly demonstrates the prevalence of the (111) and (100) planes, as identified by STM for the surface science model catalysts.[32] The concept of defined shape diminishes as the particle size decreases with the palladium crystallites of, for example, the Pd(acac)/alumina catalyst having insufficient atoms to fully define a surface plane but, rather, is dominated by corner atoms. An appreciation of these issues is essential in order to understand the variability of the vibrational spectrum for probe molecules adsorbed on such a range of surface structures.

B. Infrared spectroscopy

1. Pd(azide)/alumina

Figure 4 presents the background-subtracted diffuse reflectance spectra for CO on Pd(azide)/alumina. Sequential pulsing of CO is shown in Fig. 4(a) and 4(b) presents the infrared spectrum after warming the saturated overlayer to increasingly higher temperatures. The CO saturation spectrum has been presented elsewhere.[46] Figure 4(a) shows the spectral profile to be unchanged on increased CO exposure, leading to a relatively broadband at 1923 cm^{-1} and a sharp band at 1984 cm^{-1}. The former is assigned to μ_3 hollow-bonded CO and μ_2 bridge-bonded CO on (111) planes of the palladium particles.[15,19,20] The 1984 cm^{-1} feature is assigned to CO adsorbed on (100) facets and from CO bridge bonded to particle edge and steps, with a degree of "intensity borrowing" occurring from the bridging CO on the (111) facets.[22,34,46,50] The effective absence of linear CO at 2050–2100 cm^{-1} (Refs. 18–20) in Fig. 4(a) is particularly striking. Closer inspection of this region reveals two very weak features at 2064 and 2081 cm^{-1}, and indicates a low concentration of linear CO species to be present under these conditions. The spectra are obtained via sequential pulsing of the sample with aliquots of CO, with the sample maintained in a continuous stream of high-purity helium acting as a carrier gas, i.e., $P_{equil}CO \rightarrow 0$ torr, $P_{equil}He = 1140$ torr. This situation equates to the spectra-recorded postevacuation for the more conventional equilibrium measurements, which typically produce distinct linear (on-top) CO bands in the 2100 cm^{-1} region for Pd/Al_2O_3 catalysts.[15,42] Furthermore,

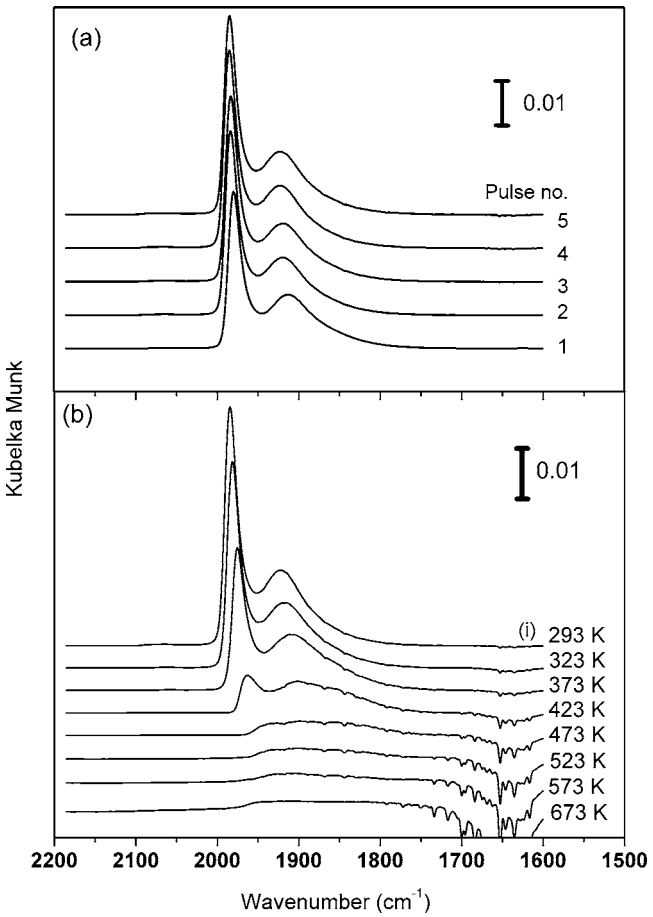

FIG. 4. (a) The diffuse reflectance infrared spectra for sequential pulsing of CO on the 7.3 wt % $Pd(azide)/Al_2O_3$ catalyst at 293 K. Pulses 1–3 correspond to an exposure of 13 μmol CO g_{cat}^{-1} $pulse^{-1}$, whereas pulses 4 and 5 correspond to an exposure of 65 μmol CO g_{cat}^{-1} $pulse^{-1}$. (b) The diffuse reflectance infrared spectrum of a saturated chemisorbed overlayer of CO as a function of temperature. (i) Saturation spectrum dosed at 293 K. The sample was then progressively warmed to 323, 373, 423, 473, 523, 573, and 673 K. A flow of He was continually passed over the sample while heating to progressively higher temperatures. The sample was held at the desorption temperature for 10 min then allowed to cool to room temperature, where the spectrum was acquired. All spectra are background subtracted, where the spectrum of the clean activated catalyst has been subtracted from the dosed spectrum.

it is noted that no linear species are normally observed for Pd single crystals, where the spectra tend to be recorded in the presence of low equilibrium pressures of CO.[21] This contrast between Pd single crystals and supported Pd catalysts shows that for extended low index planes, on-top CO cannot be populated at low partial pressures of CO,[21] however, this state is accessible under comparable conditions on small Pd crystallites.[15,19] The extent of the population of this state on the Pd crystallites is thought to be an indication of the defect density[34,42] or number of Pd sites of low coordination number.[15] Figure 4(a) has virtually zero intensity about 2100 cm^{-1}, indicating that the Pd(azide)/alumina catalyst approximates to a high surface area model catalyst, which presents a similar morphology to that of low index Pd single crystals. Specifically, the saturated CO spectrum for this catalyst resembles that expected for a combination of Pd(111) and Pd(100) single crystals.[21] In this way, this sample provides a most useful benchmark against which

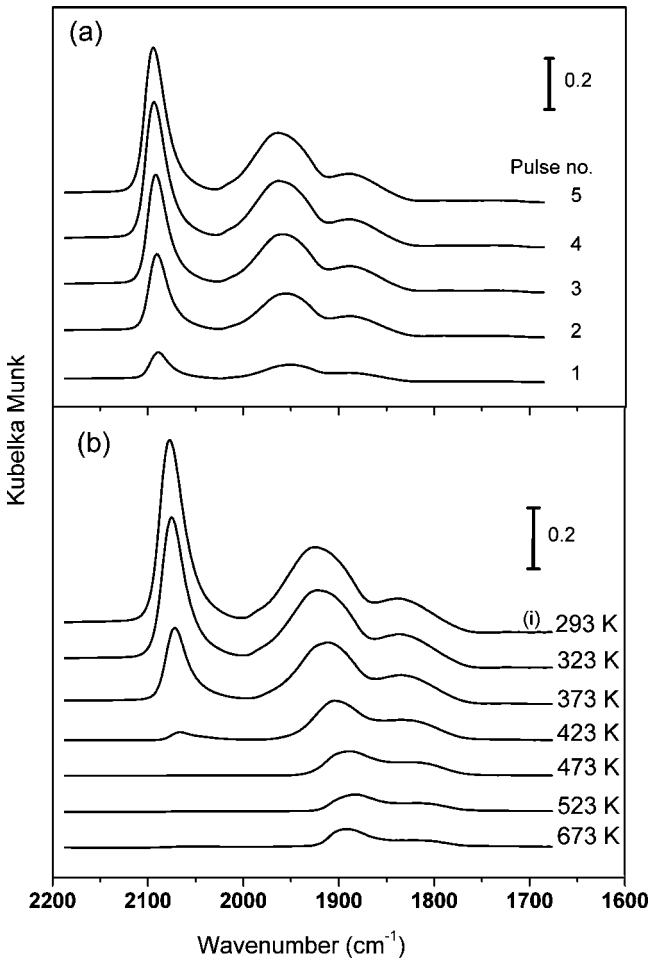

FIG. 5. (a) The background-subtracted diffuse reflectance infrared spectra for sequential pulsing of CO on the 1 wt % Pd(acac)/Al_2O_3 catalyst. Each pulse corresponds to an exposure of 13 μmol CO g_{cat}^{-1}. (b) The background-subtracted diffuse reflectance infrared spectrum of a saturated chemisorbed overlayer of CO as a function of temperature. (i) Saturation spectrum dosed at 293 K. The sample was then progressively warmed to 323, 373, 423, 473, 523, and 673 K.

other high surface area alumina-supported palladium catalysts can be evaluated. It is worthwhile noting that the linear CO state for Pd(azide)/alumina is expected to be populated to a significant degree in the presence of an overpressure of CO gas.

Figure 4(b) shows the desorption characteristics of the CO-chemisorbed overlayer, where on decreasing coverage both features are seen to shift to a lower wave number, as a result of reduced lateral interactions as the density of the overlayer is reduced.[66] The band originally at 1984 cm^{-1} shifts to 1964 cm^{-1} by 423 K and has negligible intensity at 473 K. At this temperature a broad low intensity band centerd about 1880 cm^{-1} remains, that is eventually lost by warming to 673 K. This latter feature indicates that the multiply bonded CO in the hollows of the (111) facets exhibits the higher heat of adsorption. This observation is consistent with the original observations of Eischens *et al.*[17]

2. 1% Pd(acac)/alumina

The infrared spectrum on increasing CO exposure for the 1% Pd(acac)/alumina catalyst is shown in Fig. 5(a), where the first pulse leads to the observation of three bands about 1830, 1915, and 2065 cm^{-1}. A little change in the frequency position is seen as saturation coverage is achieved, with the saturation spectrum characterized by a weak broad feature at 1838 cm^{-1}, a broadband at 1924 cm^{-1}, and a sharp, intense, and symmetric band at 2077 cm^{-1} [full width at half maximum (FWHM)29 cm^{-1}]. The spectrum is clearly different to that seen for the Pd(azide)/alumina catalyst. The 1838 cm^{-1} band is associated with a high degree of coordination and is assigned to the μ_3 bridge-bonded CO in threefold sites.[15,21,32] The band at 1924 cm^{-1} in this instance is assigned to the μ_2 bridge-bonded CO on particle edges. It is acknowledged that a band at 1923 cm^{-1} seen with the Pd(azide)/alumina catalyst has previously been assigned to bridged species on (111) facets but the difference in the particle sizes between these catalysts, Table I and illustrated in Fig. 3, means that the concept of extended planes revealed by TEM to exist on the Pd(azide) catalyst[46] is inappropriate with the much smaller Pd(acac)/alumina catalyst. Thus, it is thought that the bridging bands are partitioned between bonding on particle edges (higher frequency) and CO bonding to hollow sites (lower frequency). Unfortunately, this analysis implies that a single frequency position for a fixed coverage and adsorption temperature can be misleading with respect to the underlying crystallite morphology.

In marked contrast to the Pd(azide)/alumina catalyst, the sharp 2077 cm^{-1} band representing linear (on-top) CO[19] dominates the spectrum. This is consistent with particularly finely divided palladium particles.[15,24,25] Table I shows the mean diameter of the palladium crystallites to be 1.2 nm, which, as illustrated in Fig. 3, approximates to a particle comprised of only four palladium atoms across the diameter of an assumed sphere. Given this geometric constraint, this feature is assigned to CO linearly bound to particle corners. The narrowness of the band indicates the presence of just one type of adsorption site. Thus, despite the potential overlap of vibrational frequencies for bridged CO molecules residing in different sites mentioned above, there is a considerable contrast between the overall chemisorbed CO infrared spectrum for the Pd(azide)- and Pd(acac)-derived catalysts, which demonstrates a potentially useful sensitivity to changes in metal particle size and shape. Recent work by Bertarione *et al.* has also indicated a role for the linear CO species in reflecting the heterogeneity of supported palladium crystallites.[42]

Figure 5(b) presents the infrared spectra obtained from progressive warming of a saturated overlayer of CO. The frequency position of the linear CO band is effectively unchanged as it decreases in intensity and is removed from the spectrum after warming to 473 K. This is consistent with a single species effectively decoupled from its adjacent neighbors and is consistent with the assignment of this feature to particle corners on small palladium crystallites, as depicted in Fig. 3. In contrast, the band at 1924 cm^{-1} shifts to lower frequency on decreasing coverage, being at 1881 cm^{-1} after warming to 523 K. This frequency shift is indicative of a degree of dipolar coupling for the CO residing in these sites (μ_2 bridge-bonded CO on particle edges). Further warming to 673 K leads to a decrease in intensity but, surprisingly,

also an increase in stretching frequency to 1905 cm^{-1}. The origin of this discontinuous shift to higher frequency is unknown, although it could reflect either a degree of readsorption at these low CO coverages or possibly some agglomeration of the finely divided palladium particles. The broad feature about 1838 cm^{-1} in the saturation spectrum band exhibits a progressive decrease in intensity on increased desorption of CO from the catalyst surface. The fact that the 1838 and 1924 cm^{-1} features still have residual intensity after warming to 673 K, whereas the 2077 cm^{-1} band is lost upon warming to 473 K indicates the linear CO species to have the lower enthalpy of adsorption.

The relatively narrow linewidth and symmetric line shape of the on-top CO band at 2077 cm^{-1} is indicative of a well-defined adsorption geometry. Additionally, Fig. 5(b) shows the band shape to be retained throughout the thermal depopulation process, with no other bands apparent. The absence of defined low index planes for this size of particle (Fig. 3) means that the terms edge atom and corner atom are interchangeable for the crystallites under consideration here. Collectively, the Pd(azide)- and Pd(acac)-derived catalysts represent useful markers, against which the infrared spectra of adsorbed CO for the other catalysts can be compared.

3. 5% $Pd(NO_3)_2$/alumina

The spectra for increasing CO exposure on the 5% $P(NO_3)_2$/alumina catalyst are shown in Fig. 6(a). Two bands about 1895 and 1968 cm^{-1} are seen for the first pulse, which increase in intensity on further pulsing to give bands at 1896 and 1969 cm^{-1}, i.e., no obvious shift on increasing coverage. A linear CO species at 2079 cm^{-1} is seen from the second pulse, with the band clearly skewed to low frequency down to ca. 2000 cm^{-1}, which represents the onset of the band at 1969 cm^{-1}. The saturation spectrum, different again from that seen for the Pd(azide)/alumina (Fig. 4) and the Pd(acac)/alumina (Fig. 5) catalysts, closely resembles that reported for a number of alumina-supported palladium catalysts, e.g., Refs. 15 and 19. The 1896 cm^{-1} feature is assigned to the μ_3 hollow-bonded CO or bridged-bonded CO on (100) planes of the palladium particles[15] and the 1969 cm^{-1} band is assigned to CO adsorbed on (100) facets and from CO bridge bonded to particle edges and steps.[33,50] Although the linear CO band has a maximum at 2079 cm^{-1}, its broad shape indicates some heterogeneity in the adsorption geometries sampled by that species. Within the low-frequency tail, a band about 2050 cm^{-1} is discernible, indicating the presence of at least two types of site.

The consequences of warming a CO adlayer of the 5% $Pd(NO_3)_2$/alumina catalyst is shown in Fig. 6(b). Warming to 423 K shows disproportionate trends in the desorption profiles of the four bands discussed above. The intensity of the 1969 cm^{-1} feature is relatively unperturbed, whereas there is a substantial reduction in the intensity of the band originally at 1869 cm^{-1}. Differences are also apparent within the linear CO region of the spectrum. The 2079 cm^{-1} band disappears on warming to 423 K, leaving a single feature at 2050 cm^{-1}. This profile confirms the presence of two species of linear CO, with the lower wavenumber counterpart exhibiting a higher enthalpy of adsorption, as noted by Sheppard and Nguyen.[15] The Pd(azide)/alumina catalyst demonstrates that under these conditions linear CO will effectively not form on (111) or (100) planes (Fig. 4) and the Pd(acac)/alumina catalyst shows a sharp narrow band at 2077 cm^{-1}, which can be attributed to corner/edge atoms on very small Pd particles (Fig. 5). Thus, it appears that under the experimental conditions employed here, linear CO can only form on edge and corner atoms. More open planes or "defect sites" would presumably also permit formation of on-top CO although work by Hoffmann and co-workers on the relatively open structure of Pd(210) failed to observe any bands due to linear CO,[21] suggesting a reduced role for the former possibility. It is suggested that the spectra presented in this work can be assigned without reference to defect sites. Taking such considerations further, Figs. 3 and 6 suggest two adsorption geometries that could be responsible for the adsorption of CO in a linear form: (i) (111)/(111) and (111)/(100) edge sites and (ii) corner atoms. Figure 5 shows the linear CO band at 2077 cm^{-1} for the Pd(acac)/alumina catalyst to have fully desorbed by heating to 473 K and is assigned to CO occupying corner sites. The frequency and desorption characteristics of this feature map closely that seen for the 2079 cm^{-1} band of the 5% $Pd(NO_3)_2$/alumina catalyst seen in Fig. 6 and, therefore, this band is also assigned to linear CO resid-

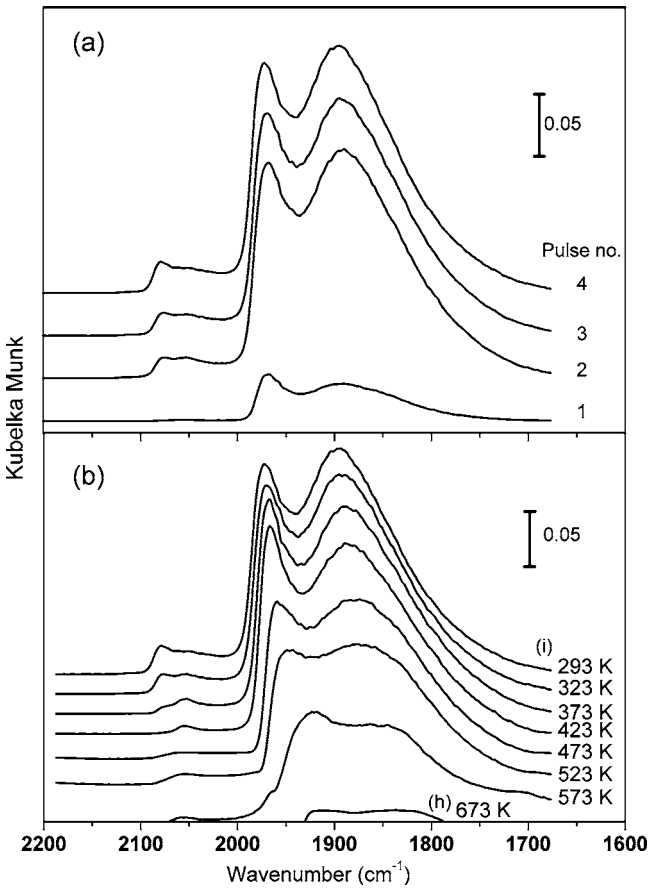

FIG. 6. (a) The background-subtracted diffuse reflectance infrared spectra for sequential pulsing of CO on the 5 wt % $Pd(NO_3)_2/Al_2O_3$ catalyst. Each pulse corresponds to an exposure of 65 μmol CO g_{cat}^{-1}. (b) The background-subtracted diffuse reflectance infrared spectrum of a saturated chemisorbed overlayer of CO as a function of temperature. (i) Saturation spectrum dosed at 293 K. The sample was then progressively warmed to 323, 373, 423, 473, 523, 573, and 673 K.

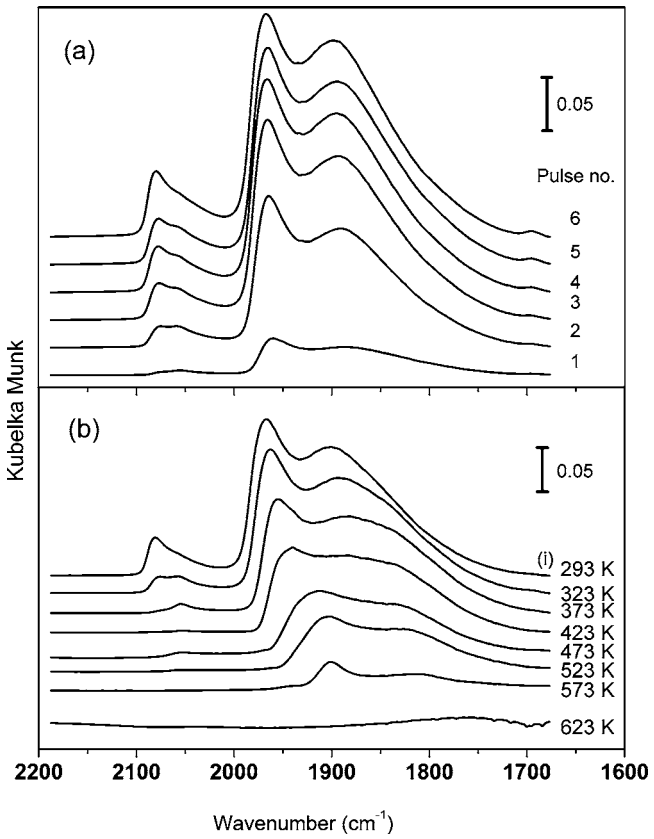

FIG. 7. (a) The background-subtracted diffuse reflectance infrared spectra for sequential pulsing of CO on the 1 wt % $Pd(NO_3)_2/Al_2O_3$ catalyst. Each pulse corresponds to an exposure of 13 μmol CO g_{cat}^{-1}. (b) The background-subtracted diffuse reflectance infrared spectrum of a saturated chemisorbed overlayer of CO as a function of temperature. (i) Saturation spectrum dosed at 293 K. The sample was then progressively warmed to 323, 373, 423, 473, 523, 573, and 673 K.

ing on corner atoms. The relatively lower intensity 2050 cm^{-1} band in Fig. 6 is then assigned to (111)/(100) and (111)/(111) edge sites. This band is present at 573 K, indicating the edge sites to exhibit a higher enthalpy of adsorption. In this way, the binding energy of this species is consistent with the observed lower vibrational frequency in terms of the Blyholder model for CO chemisorption on metal surfaces.[67] Namely, a stronger $M-CO$ bond implies a strong $CO \rightarrow Pd$ dative bond with associated back donation from the metal to the CO $2\pi^*$ molecular orbitals, which will result in a reduced C–O force constant and a lowering of the C–O stretching frequency. Thus, as is observed, the 2079 cm^{-1} band desorbs prior to the feature at 2050 cm^{-1}.

4. 1% $Pd(NO_3)_2$/alumina

The infrared spectra for the 1% $Pd(NO_3)_2$/alumina catalyst are shown in Fig. 7. The CO saturation spectrum has been published elsewhere.[46] Figure 7(a) illustrates how the spectrum develops as a function of increasing CO coverage. Four bands are discernible after the first pulse of CO at 1875, 1959, 2050, and 2074 cm^{-1}. These features develop so that the saturation spectrum is represented by (i) a broadband at 1896 cm^{-1}, which is assigned to μ_3 hollow bonded on Pd(111) planes or μ_2 bridge-bonded CO on (100) planes; (ii) a somewhat sharper band at 1969 cm^{-1} attributed to the μ_2 bridge-bonded CO on Pd(100) facets and CO bridge bonded to particle edges; (iii) a linear CO peak at 2060 cm^{-1} associated with CO bound to (111)/(111) and (111/(100)) particle edges; and (iv) a more intense linear CO band at 2079 cm^{-1} associated with CO bound to particle corners. These features are all present with the 5% $Pd(NO_3)_2$/alumina catalyst [Fig. 6(a)], although some differences in the relative intensities are apparent. In particular, the lower loading catalyst displays relatively greater intensity in the band associated with (100) facets and particle corners compared to the lower-frequency component associated with (111) planes. Additionally, the linear features relative to the bridge-bonded features are more pronounced on the 1% $Pd(NO_3)_2$/alumina catalyst, which reflects the proportionally greater contribution from particle edges and corners on reduced particle size, as depicted in Fig. 2.

Heating the saturated adlayer to 323 K confirms the existence of two linear CO peaks, which are seen to persist up to 423 K. As seen with the desorption profile for the 5% $Pd(NO_3)_2$/alumina catalyst [Fig. 6(b)], it is the lower-frequency linear feature assigned to CO at (111)/(111) and (111)/(100) edge sites that exhibits a higher enthalpy of adsorption compared to its higher wavenumber counterpart assigned to CO bound to Pd corner atoms. Figure 7(b) shows the bands at 1969 and 1898 cm^{-1} decrease in intensity and wave number with increasing temperature to yield respective peaks at 1898 and 1810 cm^{-1} after heating to 573 K. The clear base line seen in Fig. 7(b) establishes that $\Delta H_{ad}(\text{bridged}) > \Delta H_{ad}(\text{linear})$ and that all of the CO have left the surface after warming to 623 K.

5. 1% /alumina

The CO infrared spectrum for the 1% $PdCl_2$/alumina catalyst is shown in Fig. 8(a), where saturation is nearly achieved upon initial pulsing and the spectrum is defined by three bands. The 1864 cm^{-1} band is attributed to μ_3 hollow-bonded CO on Pd(111) planes, the 1980 cm^{-1} band is attributed to μ_2 bridge-bonded CO on Pd(100) facets and Pd edge sites,[32,50] and the 2090 cm^{-1} feature is associated with linearly bound CO. Although the overall profile is similar to that of the 5% $Pd(NO_3)_2$/alumina catalyst (Fig. 6), the relative intensities of the bridged CO bands are different. The relative dominance of the feature at 1864 cm^{-1} in Fig. 8(a) could be indicative of the metal particles having formed raftlike structures,[68] either during the catalyst preparation or upon CO adsorption. This band is attributed to (111) planes and previous work on the chloride-derived EuroPt-1 Pt/SiO_2 catalyst has suggested that CO chemisorption can cause spherical/cubo-octahedral particles to collapse to flat rafts comprised of predominantly (111) planes.[68] However, without a conclusive TEM analysis of the sample under adsorption conditions or complementary extended x-ray-absorption fine-structure (EXAFS) data, this remains only a speculation. A more likely explanation involves the concept of dipole coupling and intensity stealing.[66] The reduced CO adsorption capacity indicated via the adsorption isotherm (Table I) is thought to result as a consequence of a chloride residue, as detected by elemental analysis (Sec. II A), that is blocking adsorption sites. This disperses the two-dimensional net of

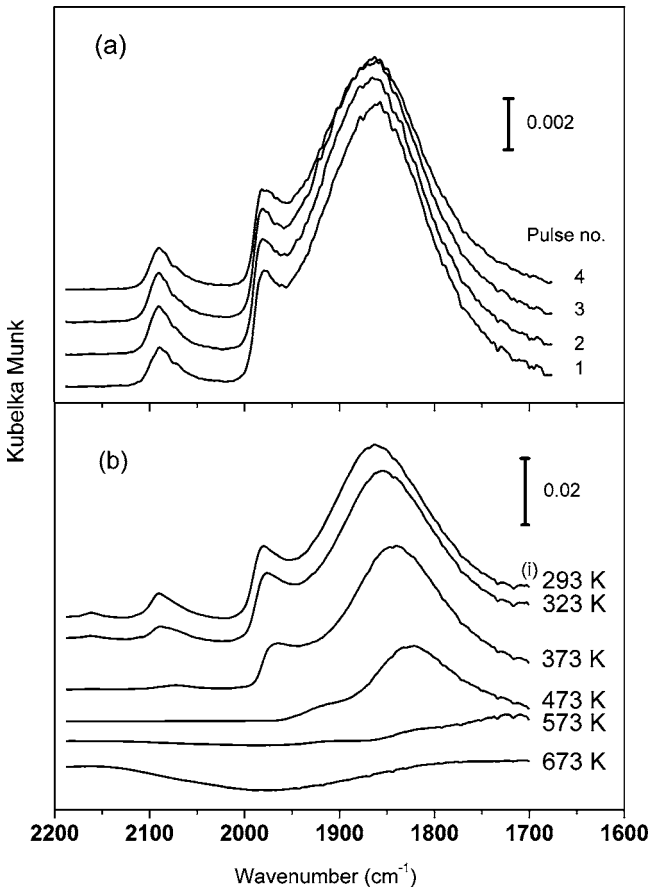

FIG. 8. (a) The background-subtracted diffuse reflectance infrared spectra for sequential pulsing of CO on the 1 wt % $PdCl_2/Al_2O_3$ catalyst. Each pulse corresponds to an exposure of 65 μmol CO g_{cat}^{-1}. (b) The background-subtracted diffuse reflectance infrared spectrum of a saturated chemisorbed overlayer of CO as a function of temperature. (i) Saturation spectrum dosed at 293 K. The sample was then progressively warmed to 323, 373, 473, 573, and 673 K.

CO molecules and thereby reduces the extent of dipole coupling and intensity stealing from the (111) band to the (100) band. These factors of dipole coupling and residue effects are a further complication that needs to be considered when using infrared spectroscopy of chemisorbed CO to probe surface morphological aspects of supported metal catalysts,[12,66] although it is noted that the Pd(azide)/alumina catalyst offers considerable potential in that regard.

This indirect evidence for the presence of chlorine residues at the metal surface helps us understand an apparent inconsistency in the chemisorption and microscopy results presented in Sec. III A. Table I shows that chemisorption predicts a mean particle size of 2.5 nm, comparable to that obtained for the 5% $Pd(NO_3)_2$ catalyst, for which metal particles are discernible in Fig. 1(a). However, no metal particles were observable for the 1% $PdCl_2$ catalyst using the same microscope and same sample preparative procedures. This contradiction can be rationalized by recognizing that the chloride residues are blocking a significant number of metal surface sites located over the whole crystallite (i.e., edge, corner, and low index planes), which leads to a lower CO chemisorption capacity that would otherwise be the case in the absence of any chlorine residues. In this manner chemisorption underestimates the total metal surface area, leading to predicted crystallite sizes larger than the actual case. Thus, the mean particle size for the 1% $PdCl_2$ catalyst should more correctly be reported as <2.5 nm. Because its actual size cannot be confirmed with the available apparatus, the 1% $PdCl_2$ catalyst representation in Fig. 3 is unaltered and corresponds to the chemisorption-derived value of 2.5 nm.

The CO desorption profile is presented in Fig. 8(b). Importantly, the linear CO band is not resolved into two peaks, indicating the presence of only a single species. Desorption of this feature is complete by 473 K, which compares favorably with that seen for the band attributed to the corner sites for the Pd(acac), 5% $Pd(NO_3)_2$, and 1% $Pd(NO_3)_2$ catalysts. Thus, this band is assigned to linear CO residing on corner atoms. The fact that only a single linear CO feature is seen is thought to indicate that the Cl atoms have decorated the (111)/(111) and (111)/(100) particle edges. The relatively high frequency of this linear CO stretching mode is thought to be due to chlorine residues withdrawing electron density from the palladium particles and hence decreasing back donation into the adsorbed CO.[69] With regard to the bridged species, desorption continues beyond 473 K, with noticeable shifts to low wavenumber. The band at 1980 cm^{-1} at saturation coverage decreases to 1920 cm^{-1} at 473 K and is removed on further heating to 573 K. The 1861 cm^{-1} saturation band reduces to 1807 cm^{-1} by 473 K. CO desorption from the catalyst is complete by 673 K.

C. Overview of CO saturation spectra

It is informative to examine the infrared spectrum for a saturation exposure of CO to the five catalysts studied. This is presented in Fig. 9 and Table II summarizes the band assignments. Inspection of Fig. 9 confirms that CO is partitioning in different ways on the five catalysts investigated. To the best knowledge of the authors, and despite a vast literature on the application of infrared spectroscopy to probe CO chemisorption on supported palladium catalysts,[15] this is thought to be the first time a systematic study has investigated a range of catalysts prepared from such a wide variety of precursor compounds. This fresh approach to a mature topic permits refinements in vibrational assignments that provide further insight into the particle shape and structure of the metal crystallites, which could play differential roles in catalytic reactions. Moreover, the Pd(azide)/alumina catalyst provides a useful reference to evaluate the possible role precursor residues could play in affecting the observed spectra of probe molecules, or even adorbates relevant to particular chemical transformations.

D. Propene hydrogenation

As an indicator for relative activity profiles, propene hydrogenation was selected as a test reaction[59] and the results for the 1% loading catalysts are presented in Fig. 10. Each catalyst displays a distinct profile. The 1% $Pd(NO_3)_2$/alumina catalyst is highly active immediately from the onset of passing the reaction mixture over the sample, with 96% propyne conversion after 1 min online. Thereafter, a gradual deactivation stage is seen, with conversion reduced to 93% at 100 min. Although the finely divided 1% Pd(acac)/alumina

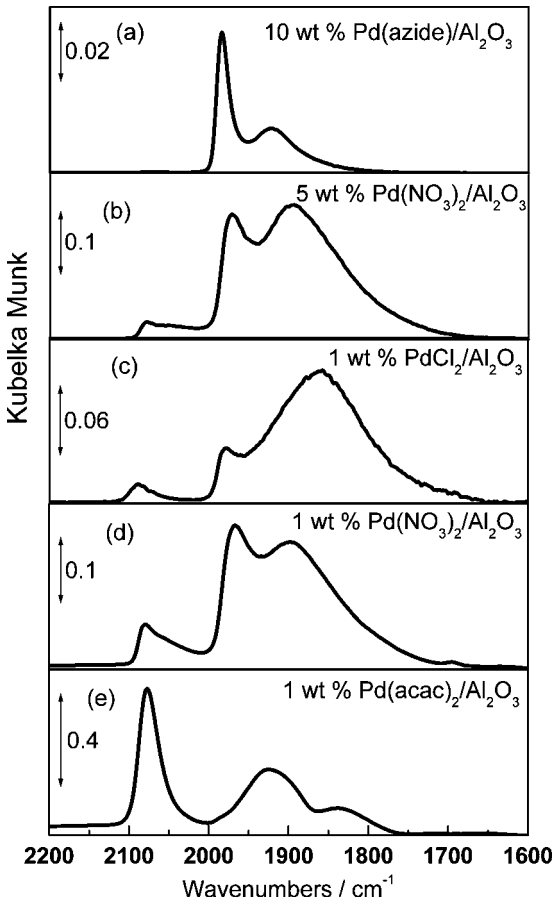

FIG. 9. Stack plot of the CO saturation diffuse reflectance infrared spectra for all five alumina-supported palladium catalysts: (a) 10% Pd(azide), (b) 5% $Pd(NO_3)_2$, (c) 1% $PdCl_2$, (d) 1% $Pd(NO_3)_2$, and (e) 1% Pd(acac). All spectra are background subtracted, where the spectrum of the clean activated catalyst has been subtracted from the dosed spectrum.

TABLE II. Summary of spectral assignments for the CO saturation spectra of the five alumina-supported Pd catalysts.

Catalyst	Vibrational frequency (cm^{-1})	Assignment
10% Pd(azide)	1923	μ_3 hollow-bonded CO and μ_2 bridge-bonded CO on (111) planes.
	1984	CO adsorbed on (100) facets and CO bridge bonded to particle edge and steps.
1% Pd(acac)	1838	μ_3 hollow-bonded CO in threefold sites.
	1924	μ_2 bridge-bonded CO on particle edges.
	2077	CO linearly bound to particle corners
5% $Pd(NO_3)_2$	1896	μ_3 hollow-bonded CO on Pd(111) or μ_2 bridge-bonded CO on (100) planes.
	1969	CO adsorbed on (100) facets and from CO bridge bonded to particle edges and steps.
	2050	Linear CO residing on (111/(111)) and (111/(100)) edge sites.
	2079	Linear CO occupying corner atom sites.
1% $Pd(NO_3)_2$	1896	μ_3 hollow-bonded on Pd(111) or μ_2 bridge-bonded CO on (100) planes.
	1969	μ_2 bridge-bonded CO on Pd(100) facets and CO bridge bonded to particle edges.
	2060	Linear CO bound to (111/(111)) and (111)/(100) particle edges.
	2079	Linear CO bound to particle corners.
1% $PdCl_2$	1864	μ_3 hollow-bonded CO on Pd(111) planes
	1980	μ_2 bridge-bonded CO on Pd(100) facets and Pd edge sites.
	2090	Linear CO residing on corner atoms.

catalyst ultimately achieves and maintains total propene conversion (100% of the incident propene molecules hydrogenated to propane) after a short period of time, a clear induction period is also evident with this catalyst. At 1 min, conversion is only 14%, which rises to 99% at a 10 min reaction time. This profile is indicative of a conditioning process that has been reported previously using pulse-flow techniques applied to propyne hydrogenation over alumina-supported palladium and platinum catalysts.[6] Interestingly, no deactivation channel is apparent over the course of the reaction period studied. In marked contrast to these samples, the 1% $PdCl_2$/alumina catalyst exhibits only modest activity. The conversion values for 1, 10, and 100 min on stream are, respectively, 10%, 16%, and 18%; considerably less than that of the other two samples. Table III relates these hydrogenation activities to the number of surface palladium atoms, as determined from CO chemisorption, and presents the associated turnover frequencies (TOF). At a 100 min time on stream the Pd(acac), $Pd(NO_3)_2$, and $PdCl_2$ catalysts exhibit respective turnover frequencies of 580, 714, and 235 propene molecules $min^{-1}\ Pd_s^{-1}$. From this series, the $Pd(NO_3)_2$/alumina catalyst provides a suitable datum, indicating a maximum turnover frequency of ca. 714 propene molecules $min^{-1}\ Pd_s^{-1}$. As the Pd(acac)/alumina catalyst is operating at 100% conversion it is only possible to state that its capacity for hydrogenating incident propene molecules under these experimental conditions exceeds 580 propene molecules $min^{-1}\ Pd_s^{-1}$. This leaves the $PdCl_2$/alumina catalyst with the lowest turnover number. Clearly it still exhibits a substantial catalytic activity for this reaction, as demonstrated by a respectable TOF; however, it is lower than that seen for the other two catalysts examined in this manner. This inferior catalytic performance is thought to be associated with chlorine residues originating

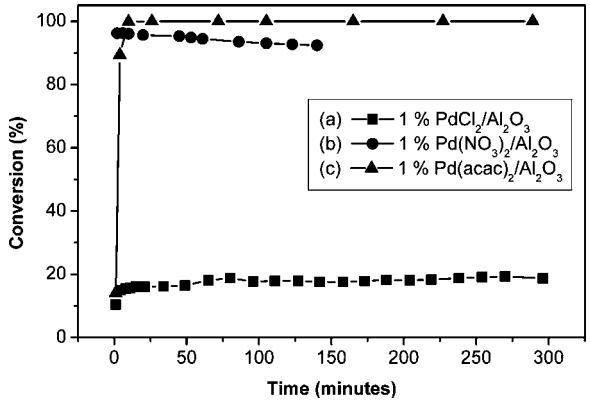

FIG. 10. Propene conversion as a function of time on stream for propene hydrogenation studies performed in a microreactor at 293 K for an equimolar mixture of hydrogen and propene: (a) 1% $PdCl_2/Al_2O_3$, (b) 1% $Pd(NO_3)_2/Al_2O_3$, and (c) 1% $Pd(acac)_2/Al_2O_3$.

TABLE III. Turnover frequencies for propene hydrogenation for the 1 wt % catalysts based on propene conversion at 100 min time on stream. The density of the surface Pd atoms is determined from CO chemisorption measurements.

Catalyst	Propene conversion at 100 min (%)	Reaction rate (propene molecules min^{-1})	$Pd_{(s)}$ (Pd atoms $g^{-1}_{(cat)}$)	TOF (propene molecules min^{-1} $Pd^{-1}_{(s)}$)
1% Pd(acac)/alumina	100	2.96×10^{20}	5.10×10^{19}	580
1% $Pd(NO_3)_2$/alumina	93	2.75×10^{20}	3.85×10^{19}	714
1% $PdCl_2$/alumina	18	5.53×10^{19}	2.35×10^{19}	235

from the precursor compound and preparative process poisoning the propene → propane conversion process.[70] The lack of activity compared to the other two supported palladium catalysts with a similar metal loading suggests that the chlorine is present at, or close to, those sites active for alkene hydrogenation. Previous work has attributed hydrocarbonaceous overlayers as being responsible for the alkyne hydrogenation activity of supported palladium catalysts.[63] The CO adsorption isotherm (Table I) and CO infrared spectrum (Fig. 8) for the $PdCl_2$/alumina catalyst reflect the accessibility of surface Pd atoms for propene and hydrogen adsorptions, therefore it is thought that the Cl residue could be perturbing the formation of the overlayer to affect the hydrogenation reaction. Section III B 5 indicated the presence of chlorine within the low index planes, as well as at the particle edges. Presumably, both of these sites play a role in the alkene hydrogenation process. The fact that the Pd(acac)/alumina catalyst maintains such a high activity indicates that corner atoms are essential. Stereochemical constraints within the hydrocarbonaceous overlayer have been used to understand selectivity issues in alkyne hydrogenations,[6,71,72] and these require defined metal surface areas that would be more associated with low index planes, rather than edge or corner sites. However, edge sites could play a vital role in hydrogen supply,[63,41] therefore the relative inactivity seen for the $PdCl_2$/alumina catalyst could quite reasonably be attributed to a reduced hydrogen supply, as a consequence of chlorine residues decorating these sites and reducing the opportunities for dissociative hydrogen adsorption.

Clearly, the elucidation of structure/activity relationships in the case of alkene hydrogenation reactions has only been explored briefly here. However, the potential for using morphological deductions using infrared spectroscopy as outlined, and applying this methodology to investigate more discerning selective hydrogenation reactions, are topics worthy of further investigation. Subsequent studies by the authors have examined all of the catalysts investigated here for the hydrogenation of crotonaldehyde.[73] That work correlates the hydrogenation susceptibility of the double-bond and aldehyde functionalities with metal morphology and indicates ways in which catalyst preparative procedures can be used to emphasize particular product distributions.

IV. CONCLUSIONS

This infrared spectroscopic investigation of CO chemisorption, achieved using pulse-flow techniques, on a series of high surface area alumina-supported palladium catalysts has refined the understanding of the link between the resulting vibrational spectra and crystallite morphology. The main conclusions can be summarized as follows:

- The Pd(azide)/alumina sample is a high surface area catalyst presenting palladium particles dominated by (111) and (100) planes that permits useful comparisons to UHV-based metal single crystal and model catalyst studies. In particular, under the conditions employed in this work, it establishes that the presence of on-top CO cannot be attributed to low index planes.
- The highly dispersed Pd(acac)/alumina catalyst indicates the contribution that corner atoms can make to the vibrational spectrum of chemisorbed CO.
- The $Pd(NO_3)_2$/alumina catalysts indicate that the linear CO species can be resolved into two features: corner atoms and edge atoms. Temperature-programmed infrared experiments reveal the low wavenumber component to exhibit the higher enthalpy of adsorption and this feature is tentatively assigned to CO bound to (111)/(111) and (111)/(100) particle edges.
- The $PdCl_2$/alumina catalyst is useful in that, as a consequence of chlorine residues remaining from the preparative procedures, the extent of dipole coupling is diluted relative to, for example, that observed for the nitrate-based catalysts. In this way, the infrared intensities of the bridge-bonded CO species more closely reflect the relative densities of the (111) and (100) facets.
- An assessment of catalyst activity has been explored by examining the 1 wt % loaded catalysts for propene hydrogenation in an equimolar hydrogen: propene mixture at 293 K in a microreactor. Each catalyst presented a different reaction profile, with the Pd(acac)/alumina and $Pd(NO_3)_2$/alumina catalysts exhibiting steady-state conversions in excess of 90%. Inspection of the associated turn-over frequencies implies that the reduced activity seen with the $PdCl_2$/alumina catalyst could be a function of a diminished hydrogen supply due to the decoration of edge sites by residual chlorine.

Further work is under way to investigate this suite of substrates for structure/reactivity relationships in gas-phase-selective hydrogenation reactions.[73]

ACKNOWLEDGMENTS

Synetix and the University of Glasgow are thanked for the award of a research studentship (TL). The Scottish Higher Education Funding Council assisted with equipment funding via a Research Development Grant. ICI are thanked for the award of a Lectureship in Heterogeneous Catalysis (DL). The Royal Society are thanked for assistance with equipment funding.

[1] M. A. Banares, Catal. Today **100**, 71 (2005).
[2] J. M. Thomas, Faraday Discuss. **105**, 1 (1996).
[3] H. Topsoe, J. Catal. **216**, 155 (2003).
[4] A. H. Adams, F. Haass, T. Buhrmester, J. Kunert, J. Ott, H. Vogel, and H. Fuess, J. Mol. Catal. A: Chem. **216**, 67 (2004).
[5] O. Shekhah, W. Ranke, and R. Schlogl, J. Catal. **225**, 56 (2004).
[6] D. R. Kennedy, G. Webb, S. D. Jackson, and D. Lennon, Appl. Catal., A **259**, 109 (2004).
[7] N. Macleod, J. R. Fryer, D. Stirling, and G. Webb, Catal. Today **46**, 37 (1998).
[8] M. Goringe, A. Rawcliffe, A. Burden, J. Hutchison, and R. Doole, Faraday Discuss. **105**, 85 (1996).
[9] A. T. Bell, in *Vibrational Spectroscopy of Molecules on Surfaces*, edited by J. T. Yates, Jr. and T. E. Madey (Plenum, New York, 1987), p. 105.
[10] V. M. Browne, S. G. Fox, and P. Hollins, Catal. Today **9**, 1 (1991).
[11] C. E. Anson, N. Sheppard, B. R. Bender, and J. R. Norton, J. Am. Chem. Soc. **121**, 529 (1999).
[12] P. C. Welch, P. S. W. Mills, C. Mason, and P. Hollins, J. Electron Spectrosc. Relat. Phenom. **64–65**, 151 (1993).
[13] R. Raval, S. F. Parker, and M. A. Chesters, Surf. Sci. **289**, 227 (1993).
[14] M. A. Chesters and D. Lennon, Surf. Sci. **426**, 92 (1999).
[15] N. Sheppard and T. T. Nguyen, Adv. Infrared Raman Spectrosc. **5**, 67 (1978).
[16] N. Sheppard and C. De la Cruz, Adv. Catal. **41**, 1 (1996).
[17] R. P. Eischens, S. A. Francis, and W. A. Pliskin, J. Phys. Chem. **60**, 194 (1956).
[18] R. F. Baddour, M. Modell, and R. L. Goldsmith, J. Phys. Chem. **74**, 1787 (1970).
[19] A. Palazov, C. C. Chang, and R. J. Kokes, J. Catal. **36**, 338 (1975).
[20] P. Gelin, A. Siedle, and J. T. Yates, Jr., J. Phys. Chem. **88**, 2978 (1984).
[21] A. M. Bradshaw, and F. M. Hoffman, Surf. Sci. **72**, 513 (1978); A. Ortega, F. M. Hoffman, and A. M. Bradshaw, *ibid.* **119**, 79 (1982).
[22] H. Unterhalt, G. Rupprechter, and H.-J. Freund, J. Phys. Chem. B **106**, 356 (2002).
[23] W. K. Kuhn, J. Szanyi, and D. W. Goodman, Surf. Sci. Lett. **274**, L611 (1992).
[24] R. van Hardeveld and F. Hartog, Adv. Catal. **22**, 75 (1972).
[25] J. K. A. Clarke, G. Farren, and H. E. Rubalcava, J. Phys. Chem. **71**, 2376 (1967).
[26] F. Figueras, R. Gomez, and M. Primet, Adv. Chem. Ser. **121**, 480 (1973).
[27] J. L. Lemaitre, P. G. Menon, and F. Delanny, *Characterisation of Heterogeneous Catalyst* (Marcel Dekker, New York, 1984), p. 299.
[28] R. W. Judd, H. J. Allen, P. Hollins, and J. Pritchard, Spectrochim. Acta, Part A **43**, 1607 (1987).
[29] E. H. Voogt, L. Coulier, O. L. J. Gijzeman, and J. W. Gues, J. Catal. **169**, 359 (1997).
[30] D. R. Rainer, C. Xu, and D. W. Goodman, J. Mol. Catal. A: Chem. **119**, 307 (1997).
[31] T. Schroeder, M. Adelt, B. Richter, N. Naschitzki, M. Bäumer, and H.-J. Freund, Surf. Rev. Lett. **7**, 7 (2000).
[32] M. Bäumer and H.-J. Freund, Prog. Surf. Sci. **61**, 127 (1999).
[33] M. Frank and M. Bäumer, Phys. Chem. Chem. Phys. **2**, 3723 (2002).
[34] K. Wolter, O. Seiferth, H. Kuhlenbeck, M. Bäumer, and H.-J. Freund, Surf. Sci. **399**, 190 (1998).
[35] I. Stará and V. Matloín, Surf. Sci. **313**, 99 (1994).
[36] I. Jungwirthová, I. Stará, and V. Matloín, Surf. Sci. **377–379**, 644 (1997).
[37] Sh. Shaikhutdinov, M. Heemeier, M. Bäumer, T. Lear, D. Lennon, R. J. Oldman, S. D. Jackson, and H.-J. Freund, J. Catal. **200**, 330 (2001).
[38] S. Schauermann, J. Hoffmann, V. Johánek, J. Hartmann, J. Libuda, and H.-J. Freund, Angew. Chem., Int. Ed. **41**, 2532 (2002).
[39] G. Rupprechter and H.-J. Freund, Top. Catal. **14**, 3 (2001).
[40] G. Rupprechter, Phys. Chem. Chem. Phys. **3**, 4621 (2001).
[41] M. Morkel, G. Rupprechter, and H.-J. Freund, Surf. Sci. Lett. **588**, L209 (2005).
[42] S. Bertarione, D. Scarano, A. Zecchina, V. Johánek, J. Hoffmann, S. Schauermann, M. M. Frank, J. Libuda, G. Rupprechter, and H.-J. Freund, J. Phys. Chem. B **108**, 3603 (2004).
[43] S. Bertarione, D. Scarano, A. Zecchina, V. Johánek, J. Hoffmann, S. Schauermann, M. M. Frank, J. Libuda, G. Rupprechter, and H.-J. Freund, J. Catal. **223**, 64 (2004).
[44] C. N. Satterfield, *Heterogeneous Catalysis in Industrial Practice*, 2nd ed. (Krieger, Malabar, FL, 1996), p. 114.
[45] R. J. Farrauto and C. H. Bartholomew, *Fundamentals of Industrial Catalytic Processes* (Blackie, London, 1997), p. 60.
[46] T. Lear, R. Marshall, E. K. Gibson, T. Schütt, T. M. Klapötke, G. Rupprechter, H.-J. Freund, J. M. Winfield, and D. Lennon, Phys. Chem. Chem. Phys. **7**, 565 (2005).
[47] B. M. Weckhuysen, Phys. Chem. Chem. Phys. **5**, 4351 (2003).
[48] W. Beck, T. M. Klapötke, J. Knizek, H. Nöth, and T. Schütt, Eur. J. Inorg. Chem. **1999**, 523.
[49] J. Meyer, P. Neugebauer, and M. Steigerwald, Patent PCT Int. Appl. 03/014021 (2003).
[50] I. V. Yudanov *et al.*, J. Phys. Chem. B **107**, 255 (2003).
[51] V. V. Kaichev, I. P. Prosvirin, V. I. Bukhtiyarov, H. Unterhalt, G. Rupprechter, and H.-J. Freund, J. Phys. Chem. B **107**, 3522 (2003).
[52] M. Caravati, J. D. Grunwaldt, and A. Baiker, Phys. Chem. Chem. Phys. **7**, 278 (2005).
[53] E. Opara, D. T. Lundie, T. Lear, I. W. Sutherland, S. F. Parker, and D. Lennon, Phys. Chem. Chem. Phys. **6**, 5588 (2005).
[54] I. Stará and V. Matoín, Surf. Sci. **313**, 99 (1994).
[55] V. Johánek, I. Stará, N. Tsud, K. Vetruska, and V. Matoín, Appl. Surf. Sci. **162–163**, 679 (2000).
[56] G. Rupprechter, H. Unterhalt, M. Morkel, P. Galletto, L. Hu, and H.-J. Freund, Surf. Sci. **502–503**, 109 (2002).
[57] G. Rupprechter, H. Unterhalt, M. Morkel, P. Galletto, T. Dellwig, and H.-J. Freund, Vacuum **71**, 83 (2003).
[58] V. V. Kaichev, M. Morkel, H. Unterhalt, I. P. Prosvirin, V. I. Bukhtiyarov, G. Rupprechter, and H.-J. Freund, Surf. Sci. **566–568**, 1024 (2004).
[59] J. W. Yoo, D. J. Hathcock, and M. A. El-Sayed, J. Catal. **214**, 1 (2003).
[60] D. Lennon, D. R. Kennedy, G. Webb, and S. D. Jackson, Stud. Surf. Sci. Catal. **126**, 341 (1999).
[61] T. Lear, Ph.D. thesis, University of Glasgow, 2003.
[62] H. Dropsch and M. Baerns, Appl. Catal., A **158**, 163 (1997).
[63] D. Lennon, R. Marshall, G. Webb, and S. D. Jackson, Stud. Surf. Sci. Catal. **130**, 245 (2000).
[64] J. S. Smith, P. A. Thrower, and M. A. Vannice, J. Catal. **56**, 236 (1979).
[65] S. Schimpf, M. Lucas, C. Mohr, U. Rodemerck, A. Brückner, J. Radnik, H. Hofmeister, and P. Claus, Catal. Today **72**, 63 (2002).
[66] P. Hollins, Surf. Sci. Rep. **16**, 51 (1992).
[67] G. Blyholder, J. Chem. Phys. **68**, 2772 (1964).
[68] N. Sheppard and C. De La Cruz, Spectrochim. Acta, Part A **50**, 271 (1994).
[69] M. Primet, M. Dufaux, and M. V. Mathieu, C. R. Acad. Sci., Paris, Series. C, **t.280**, 419 (1975).
[70] F. A. Gracie, J. T. Miller, A. J. Kropf, and E. E. Wolf, J. Catal. **209**, 341 (2002).
[71] A. Borodzinski, Catal. Lett. **63**, 35 (1999).
[72] R. Marshall, G. Webb, S. D. Jackson, and D. Lennon, J. Mol. Catal. A: Chem. **226**, 227 (2005).
[73] T. Lear, A. R. McInroy, A. Uhl, E. K. Gibson, S. D. Jackson, T. M. Klapötke, S. Shaikhutdinov, G. Rupprechter, H.-J. Freund, and D. Lennon (to be published).